Bulletin of the Seismological Society of America, Vol. 98, No. 3, pp. 1482–1494, June 2008, doi: 10.1785/0120060159

Real-Time Evolutionary Earthquake Location for Seismic Early Warning

by Claudio Satriano, Anthony Lomax, and Aldo Zollo

Abstract An effective early-warning system must provide probabilistic estimates of the location and size of a potentially destructive earthquake within a few seconds after the event is first detected.

In this work we present an evolutionary, real-time location technique based on an equal differential time (EDT) formulation and a probabilistic approach for describing the hypocenter estimation. The algorithm, at each timestep, relies on the information from triggered arrivals and not-yet-triggered stations. With just one recorded arrival, the hypocentral location is constrained by the Voronoi cell around the first triggering station constructed using the travel times to the not-yet-triggered stations. With two or more triggered arrivals, the location is constrained by the intersection of the volume defined by the Voronoi cells for the remaining, not-yet-triggered stations and the EDT surfaces between all pairs of triggered arrivals. As time passes and more triggers become available, the evolutionary location converges to a standard EDT location.

Synthetic tests performed using the geometry of the Irpinia seismic network, southern Italy (ISNet), and the simulation of an evolutionary location for the 2000 M_w 6.6 Western Tottori, Japan, earthquake indicate that when a dense seismic network is available, reliable location estimates suitable for early-warning applications can be achieved after 1–3 sec from the first event detection. A further simulation with an M_w 6.7 southern Greece earthquake shows that at a regional scale, the real-time location can provide useful constraints on the earthquake position several seconds before a non-real-time algorithm. Finally, we show that the robustness of the algorithm in the presence of outliers can be effectively used to associate phase arrivals coming from events occurring close in time, and we present a preliminary algorithm for event detection.

Introduction

Destructive *S* and surface waves from a large earthquake can take several tens of seconds to travel from the earthquake source region to distant populated areas and sensitive infrastructure. If there is a seismological monitoring network in the source region, modern seismological analysis methods and communications systems allow characterization of the event and the issuing of alarm messages within seconds, leaving tens of seconds for mitigating actions to be taken. This procedure is known as early warning (Heaton, 1985; Lee and Espinosa-Aranda, 2003; Kanamori, 2005). For example, for an earthquake in the Irpinia region of southern Italy, there is a delay of about 25–30 sec before the first energetic *S*-wave trains arrive at Naples at about 80–100-km distance. With an early-warning system, alarm messages could be sent to critical sites in Naples 20 or more seconds before the commencement of strong shaking (Zollo *et al.*, 2006).

The characterization of an earthquake for early warning includes most importantly estimates of its location and size (Allen and Kanamori, 2003). Here we are concerned with obtaining the best possible constraint on the location of an event hypocenter as time passes after the first triggered arrival from the event. This constraint is expressed as a probability density function (PDF) for the hypocenter location in 3D space. This optimal, time-evolving, probabilistic location information will form a critical part of early-warning messages, allowing actions to be taken based on the range of likely source distances and directions as estimated at the time of each message (Iervolino *et al.*, 2006).

There are many methodologies for standard earthquake location performed when most or all the phase arrival times for an event are available. Our real-time location methodology is based on the equal differential time (EDT) formulation (Font *et al.*, 2004; Lomax, 2005) for standard earthquake location. EDT is a generalization of the master-station method (Zhou, 1994) and the method of hyperbolas cited by Milne (1886). The EDT location is given by the point traversed by the maximum number of quasi-hyperbolic surfaces, on each of which the difference in calculated travel time to a pair of stations is equal to the difference in observed arrival times for

the two stations. The EDT location determination is independent of origin time and reduces to a 3D search over latitude, longitude, and depth. Furthermore, EDT is highly robust in the presence of outliers in the data (Lomax, 2005). This robustness is critical for the present problem, because we will often work with small numbers of data and may have outlier data such as false triggers, picks from other events, and misidentified picks from energetic secondary phases.

Previous work on earthquake location for early warning includes several novel approaches to gain constraint on the location at an earlier time and with fewer observations than for standard earthquake location. Horiuchi *et al.* (2005) combine standard L_2-norm event location, EDT location on quasi-hyperbolic surfaces, and the information from not-yet-arrived data to constrain the event location beginning when there are triggered arrivals from two stations. The two arrivals times define a hyperbolic surface, which contains the event location. This solution is further constrained by EDT surfaces constructed using the current time (t_{now}) as a substitute for future unknown arrival times at the stations that have not-yet-recorded arrivals. The constraint increases as t_{now} progresses, even if no further stations record an arrival. Rydelek and Pujol (2004), applying the approach of Horiuchi *et al.* (2005), show that useful constraint on an event location can be obtained with only two triggered stations. Cua and Heaton (2007) generalized the approach by Rydelek and Pujol in order to start the location with one single-triggering station.

Method and Algorithm

Our location methodology is related to that of Horiuchi *et al.* (2005), which we extend and generalize by (1) starting the location procedure after only one station has triggered, (2) using the EDT approach throughout to incorporate the triggered arrivals and the not-yet-triggered stations, (3) estimating the hypocenter probabilistically as a PDF instead of as a point, and (4) applying a full nonlinearized global search for each update of the location estimate.

We assume that a seismic network has known sets of operational and nonoperational stations (Fig. 1a) that, when an earthquake occurs, triggers (*P*-wave arrival picks) will become available from some of the operational stations and that there may be outlier triggers, which are not due to *P* arrivals from the earthquake of interest. We consider N operational stations ($S_0, \ldots, S_N$), a gridded search volume V containing the network and target earthquake source regions, and the travel times from each station to each grid point (i, j, k) in V computed for a given velocity model.

The standard EDT approach (Font *et al.*, 2004) is based on the relation that, if the hypocenter (i, j, k) is exactly determined, the difference between calculated travel times tt_n and tt_m from the hypocenter to two stations S_n and S_m is equal to the difference between the observed arrival times t_n and t_m at the two stations, because the observed arrival times share the common earthquake origin time

$$(tt_m - tt_n)_{i,j,k} = t_m - t_n; \qquad m \neq n. \tag{1}$$

For a constant velocity model, this equation defines a 3D hyperbolic surface whose symmetry axis goes through the two stations. Given N triggering stations, $N(N-1)/2$ surfaces can be drawn, and the hypocenter will be located in the small region crossed by the maximum number of EDT surfaces.

Following an evolutionary approach, we evaluate at each timestep the EDT equations considering not only each pair of triggered stations, but also those pairs where only one station has triggered.

Therefore, when the first station S_n triggers with an arrival at $t_{\text{now}} = t_n$ (t_{now} is the current clock time), we can already place some limit on the hypocenter position (Fig. 1b). These limits are given by EDT surfaces defined by the condition that each operational but not-yet-triggered station S_l will trigger at a time $\tilde{t}_l$ in the next time instant or later (i.e., $\tilde{t}_l \geq t_n$). From equation (1),

$$(tt_l - tt_n)_{i,j,k} \geq 0; \qquad l \neq n. \tag{2}$$

The equality in equation (2) defines a conditional EDT surface, the locus of points where the *P* travel time to the first triggering station tt_n is equal to the travel time to each of the not-yet-triggered stations, tt_l, $l \neq n$. The inequality in equation (2) identifies a region of the search volume that must contain the hypocenter. For a homogeneous medium with constant *P*-wave speed, the volume bounded by the conditional EDT surfaces for all the stations at $t_{\text{now}} = t_n$ defines the Voronoi cell (Weisstein, 1999) associated to the station S_n.

As the current time t_{now} progresses, we gain the additional information that the not-yet-triggered stations S_l can only trigger with $\tilde{t}_l > t_{\text{now}}$. Thus, the hypocentral volume is bounded by conditional EDT surfaces that satisfy the inequality

$$(tt_l - tt_n)_{i,j,k} \geq t_{\text{now}} - t_n. \tag{3}$$

The system (3) defines the volume, bounded by the conditional EDT surfaces, in which the hypocenter may be located given that, at current time t_{now}, only the station S_n has triggered. If $t_{\text{now}} = t_n$, the system (3) reduces to the system (2); for $t_{\text{now}} > t_n$, the hypocentral volume will be smaller than the previous one, because the updated, conditional EDT surfaces tend to fold towards and around the first triggered station (Fig. 1c).

We interpret the hypocentral volume in a probabilistic way by defining, for each inequality in (3), a value $p_{n,l}(i, j, k)$, which is 1 if the inequality is satisfied and 0 if not. Then we sum the $p_{n,l}(i, j, k)$ over stations l at each grid point, obtaining a nonnormalized probability density $P(i, j, k)$, where $P(i, j, k) = N - 1$ for grid points where all the inequalities are satisfied and a value less than $N - 1$ elsewhere.

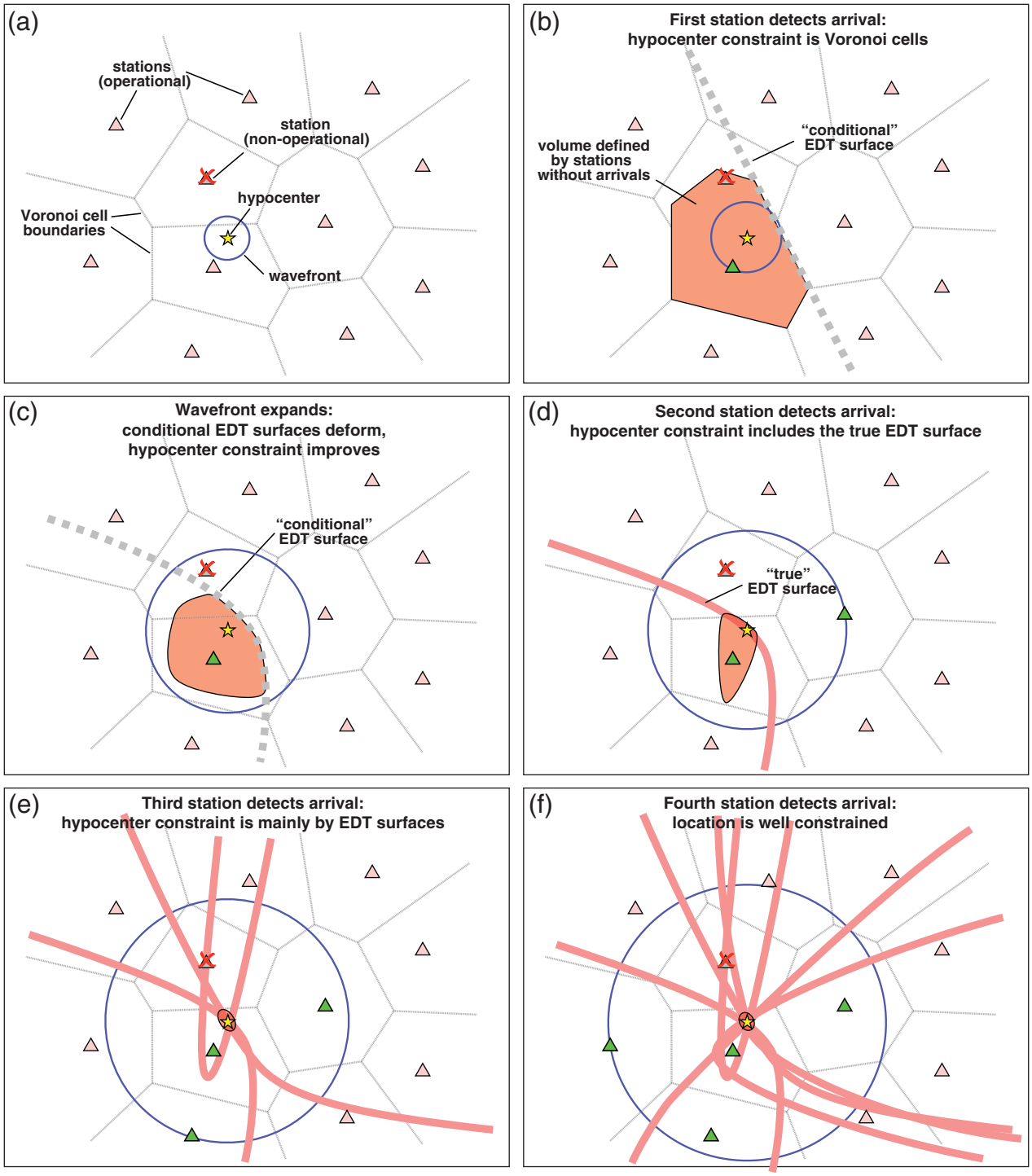

Figure 1. Schematic illustration of the evolutionary earthquake location algorithm. For clarity, only a map view with the epicentral location is represented. (a) Given a seismic network with known sets of operational and nonoperational stations, the Voronoi cell associated to each station is known *a priori*. (b) When the first station triggers, we can define a volume that is likely to contain the location; this volume is limited by conditional EDT surfaces on which the *P* travel time to the first triggering station is equal to the travel time to each of the operational but not-yet-triggered stations. (c) As time progresses, we gain additional information from the stations that have not yet triggered, the EDT surfaces move towards and bend around the first triggering station, and the likely location volume decreases in size. (d) When the second station triggers, it is possible to define a true EDT surface; the hypocenter is on the intersection between this surface and the volume defined by the conditional EDT surfaces, which continues decreasing in size. (e) When a third station triggers, two more true EDT surfaces can be drawn, further increasing the constraint on hypocenter position. (f) As more stations trigger, the location converges to the standard EDT location composed entirely of true EDT surfaces.

When the second and later stations trigger, we first reevaluate the system (3) for all possible pairs consisting of a triggered station S_n and a not-yet-triggered station S_l. Second, we construct standard, true EDT surfaces (equation 1) between each pair S_n, S_m of the triggered stations, by evaluating for each grid point the quantity

$$q_{n,m}(i,j,k) = \exp\left\{-\frac{[(tt_n - tt_m)_{i,j,k} - (t_n - t_m)]^2}{2\sigma^2}\right\}; \quad n \neq m. \tag{4}$$

The expression between square brackets in the exponent is the standard EDT equation (1) whose solutions are quasi-hyperbolic surfaces; in practice, all true EDT surfaces are given a finite width by including the uncertainty σ in the arrival time picking and the travel-time calculation.

The quantity $q_{n,m}(i,j,k)$ has values between 0 and 1. We sum the $q_{n,m}(i,j,k)$ with the $p_{n,l}(i,j,k)$ obtained from the reevaluation of (3) to obtain a new $P(i,j,k)$. The maximum value of P is

$$P_{\max} = (N - n_T)n_T + n_T(n_T - 1)/2, \tag{5}$$

where n_T is the number of stations that have triggered. The first term in (5) counts the number of inequalities from (3) and the second term, the number from (4).

Starting from P, we define a value

$$Q(i,j,k) = \left(\frac{P(i,j,k)}{P_{\max}}\right)^N, \tag{6}$$

which forms a relative PDF (with values between 0 and 1) for the hypocenter location within the grid cell (i,j,k). The function $Q(i,j,k)$ may be arbitrarily irregular and may have multiple maxima.

At predetermined time intervals, we evaluate equations (3) and (4) to obtain $Q(i,j,k)$ in the search volume, using the Oct-tree importance sampling algorithm (Lomax and Curtis, 2001; Lomax, 2005; www.alomax.net/nlloc/octtree, last accessed March 2008). This algorithm uses recursive subdivision and sampling of rectangular cells in 3D space to generate a cascade structure of sampled cells, such that the spatial density of sampled cells follows the target function values (i.e., equation 6). The Oct-tree search is much faster than a simple or nested grid search (factor 10–100 faster) and more global and complete than stochastic search methods algorithms such as simulated annealing and genetic algorithms (Lomax and Curtis, 2001). For each grid point, an origin time estimate can be obtained from the observed arrival times and the calculated travel times.

As more stations trigger, the number of not-yet-triggered stations becomes small, and the location converges towards the hypocentral volume that is obtained with standard EDT location using the full set of data from all operational stations (Fig. 1d–f).

If there are uncorrelated outlier data (i.e., triggers that are not compatible with P arrivals from a hypocenter within or near the network), then the final hypocentral volume will usually give an unbiased estimate of the hypocentral location, as with standard EDT location. However, if one or more of the first arrival times is an outlier, then the earliest estimates of the hypocentral volume may be biased. If N_{out} is the number of outlier data, the bias should be small after about $4 + N_{\text{out}}$ arrivals have been obtained and should decrease further with further arrivals as the solution converges towards a standard EDT location.

At each time interval, an alarm message can be sent with information on the current constraint on the hypocentral location. This information may include, for example, the grid point where $Q(i,j,k)$ is maximal (the maximum-likelihood hypocenter), an uncertainty on the location given by the largest horizontal and vertical distances between cells where $Q(i,j,k) > \alpha Q$ and α is a constant < 1, or a more complete representation of the PDF derived from $Q(i,j,k)$. For message recipients at specific localities, the hypocentral location, uncertainty, PDF, or other information in the alarm message can be provided as functions of epicentral distance and azimuth to the locality.

Synthetic Earthquake-Location Tests

In order to evaluate the accuracy and the robustness of the location technique, we conducted several synthetic tests using the geometry of the ISNet, a high-density, high-dynamic seismic network deployed in the region of the 1980 M_w 6.9 Irpinia earthquake (Weber *et al.*, 2007). For each simulated event, we computed synthetic arrival picks using travel times obtained by the finite difference solution of the eikonal equation (Podvin and Lecomte, 1991) for a 1D, *P*-wave velocity model (Table 1). To reproduce uncertainties introduced by the picking algorithm, we add to each arrival time a random error following a Gaussian distribution with a variance of 0.02 sec.

Here we use P picks only because currently most networks have poor capability to perform real-time S picking. Most S detection algorithms depend on the identification of a P arrival that can be associated with a possible S pick, and many S pickers use polarization information, which requires three-component analysis and introduces processing delays and inefficiencies (e.g., Magotra *et al.*, 1987; Cichowicz,

Table 1

P-Wave Velocity Model for the Irpinia Region

Depth (km)	V_p (km/sec)
0.0	2.0
1.0	3.2
2.5	4.5
15.0	6.2
35.0	7.4
40.0	8.0

1993; Withers *et al.*, 1998). We do not yet know if reliable *S* picks will be available for real-time location for ISNet and for similar scale networks. We also note that *S* picking may be difficult to impossible for larger events with long duration, emerging arrivals, and otherwise complicated waveforms, and that some *P* picks may be misidentified *S* arrivals, particularly for smaller events.

Event inside the Network

Our first test considers an earthquake occurring at the center of the network at a depth of 10 km (Fig. 2). Each panel in Figure 2 is a snapshot at a given time showing three maps for the marginal probability (i.e., summed over x, y, or z) for $Q(i, j, k)$ along the horizontal and the two vertical planes. For instance, the horizontal map represents the quantity

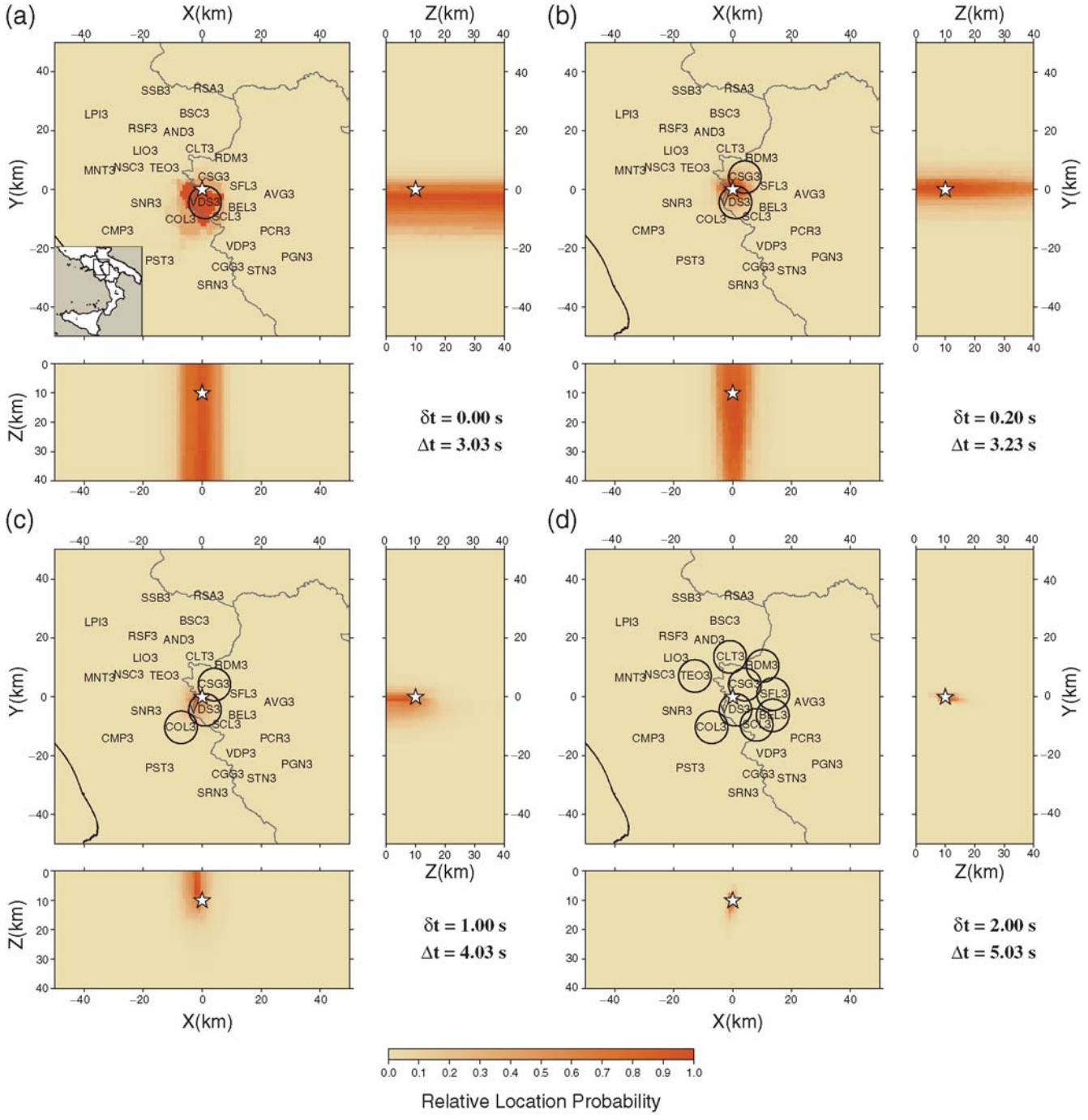

Figure 2. Location test for a synthetic event occurring at the center of the Irpinia Seismic Network (ISNet), southern Italy. The three orthogonal views show marginal values of the relative location PDF $Q(i, j, k)$ (equation 6). The true hypocenter is identified by a star. The time from the first trigger is indicated as δt, while Δt is the time from event origin. For each snapshot, stations that have triggered are marked with a circle.

$$Q_{i,j}(i,j) = \alpha \sum_k Q(i,j,k)\Delta_k,$$

where Δ_k is the grid spacing along the vertical direction (k) and α is a normalization constant, so that $Q_{i,j}(i,j)$ ranges between 0 and 1.

The star on each map shows the known synthetic hypocentral location.

The initial snapshot is taken when the first station, VDS3, triggers ($\delta t = 0$ sec) 3.03 sec (Δt) after the event origin time: the constraint on the earthquake location is given only by the probability density $Q(i,j,k)$ defined from the evaluation of equation (3) for station VDS3 against all the other not-yet-triggered stations; the epicenter is constrained within about 10 km, but depth is unconstrained. A second station (CSG3) triggers 0.20 sec later: the location PDF is now constrained by the volume defined by equation (3) and the EDT surface defined by equation (4). One second after the first trigger ($\delta t = 1$ sec, $\Delta t = 4.03$ sec), with three triggered stations, the PDF has tightened considerably, providing an estimation of the epicentral position within a few kilometers and greatly reducing the uncertainty on depth. Two seconds after the first trigger (5.03 sec from the event origin), nine stations have triggered, and the location is well constrained.

In both the examples we used an initial subdivision of the search grid, whose size is $100 \times 100 \times 40$ km, in $10 \times 10 \times 4$ cells. We then allow the Oct-tree algorithm to further subdivide the cells with highest probability value, setting the minimum allowed cell size to 0.5 km and the maximum allowed number of cells to 10,000.

The computation time increases linearly with the total number of cells evaluated, which, in turn, depends mainly on the size of the initial search grid. The optimal size of the initial search grid increases for increasing size of the search region; the minimum allowed cell size should be much less than the lesser of the average station spacing or the typical distance to the target warning site.

Our current implementation of the algorithm takes about 0.5 sec for the computation of each snapshot. It is therefore possible to perform a real-time location with a timestep of 1 sec. This is appropriate for the ISNet where packetized data is received with a time frame of 1 sec (Weber *et al.*, 2007).

Event outside the Network

Figure 3 shows a location test for an earthquake occurring outside the network at a depth of 10 km.

At $\delta t = 0$ sec, the location PDF volume is bounded only towards the network. The trigger from a second station at $\delta t = 0.80$ sec greatly improves the bounds on the location PDF, though the PDF remains elongated toward the triggered stations. Two seconds after the first trigger, with four triggered stations, the size and elongation of the PDF are reduced, and the constrain on depth improves. At $\Delta t = 8.40$ sec, 3 sec after the first event detection, and with eight triggered stations, a good epicentral location is achieved. The event depth is constrained only by a lower bound, but the depth range includes the true value.

Missed Triggers

To test how the algorithm performs when an operating station does not detect the event, we examined the case where the first or the second station does not trigger. This is the most problematic circumstance, because the very first stations have a large influence on the initial location.

Starting from the synthetic location for the event inside the network (Fig. 2), we simulated the possibility that the first (VDS3) or the second (CSG3) station did not recognize the arrival. The results are shown in Figure 4. On the left side, the case in which the first station (VDS3) does not trigger is analyzed. For simplicity, only map views of the location PDF are plotted. The initial ($\delta t = 0.20$ sec) maximum location probability is assigned to the Voronoi cell associated to station CSG3, while the actual epicenter is at the boundary of this cell. However, because the second triggering station (COL3, at $\delta t = 1.00$ sec) is on the opposite side, respect to the epicenter, the location bias is quickly removed. A third triggering station (CLT3, at $\delta t = 1.20$ sec), on the same side of CSG3 reintroduces a small bias, which is definitively removed when the fourth and the fifth stations trigger (SFL3 and SCL3, at $\delta t = 1.40$ sec, not shown in the figure).

If the first station triggers correctly, but the second does not (Fig. 4b), then, after 1 sec, the maximum location PDF is shifted between the two triggered stations (VDS3 and COL3), southwest from the actual epicenter. As soon as a station on the northern side (CLT3, at $\delta t = 1.20$ sec) triggers, the location estimate improves. Again, the bias is completely removed when the fourth and the fifth stations trigger.

Simulated Real-Time Locations for Real Earthquakes

We performed two real-time location simulations with actual recordings, using data collected at a dense seismic network (Tottori, 2000), with a station-event geometry comparable to the ISNet, and at a coarser network (southern Greece, 2006), where the mean station spacing is an order of magnitude greater than the ISNet.

Real-Time Location in a Dense Seismic Network: The 2000 Western Tottori Earthquake (M_w 6.6)

The western Tottori earthquake (M_w 6.6) occurred in southwestern Japan on 6 October 2000 (Fukuyama *et al.*, 2003); it was recorded by several permanent seismic networks, including the strong-motion networks K-Net (www.k-net.bosai.go.jp/, last accessed March 2008) and KiK-Net (www.kik.bosai.go.jp/, last accessed March 2008). We selected 25 stations from these two networks located within 50 km from the epicenter to reproduce a station distribution similar to that of ISNet.

First *P* arrivals have been determined using an automatic picker based on the evaluation of the ratio between the short

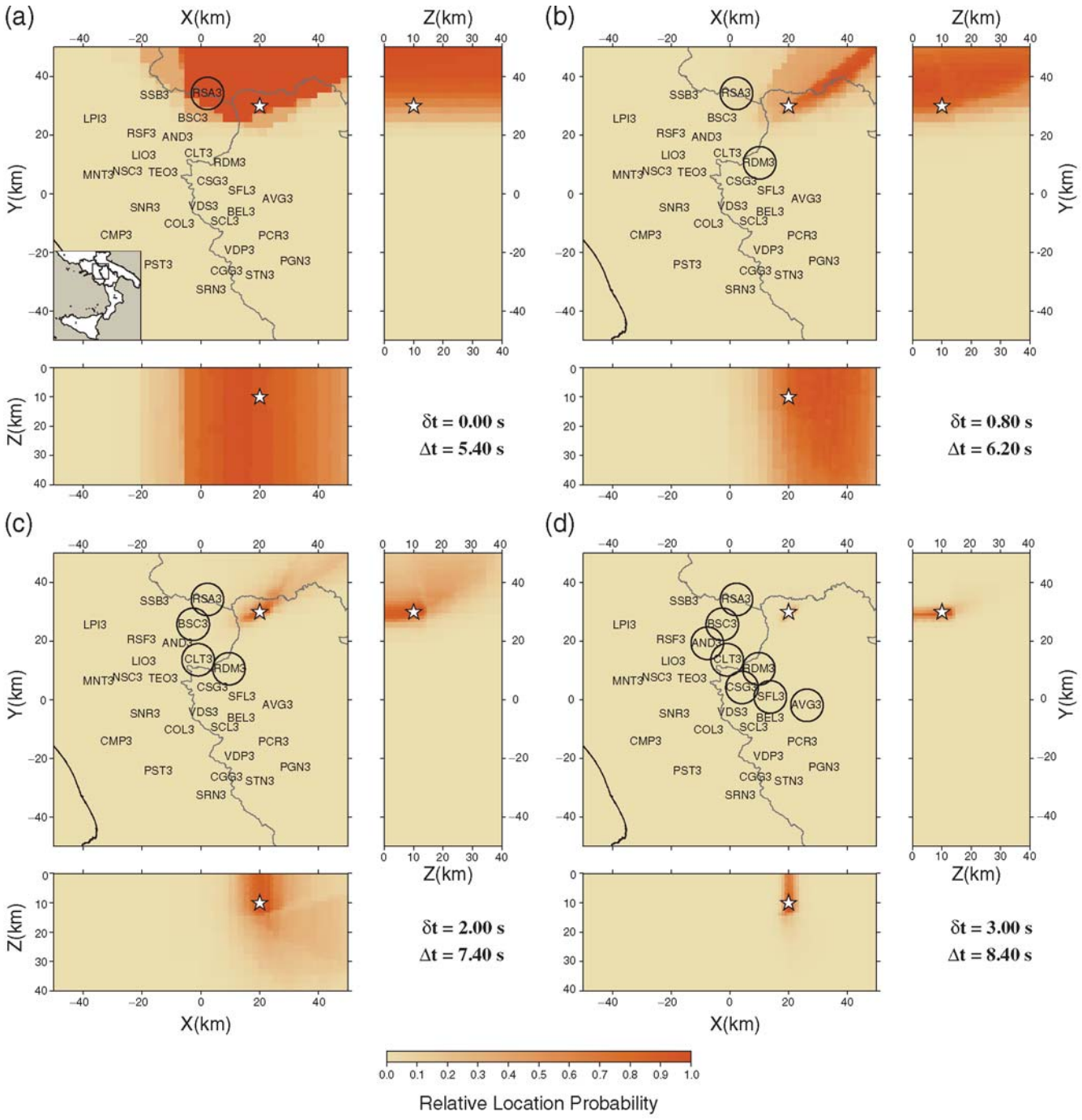

Figure 3. Location test for a synthetic event occurring outside the network (see Fig. 2 for explanation).

term average and the long term average of the signal (Allen, 1982) without any *a posteriori* review of the picked phases. We used for the location the same velocity model proposed by Fukuyama *et al.* (2003). No *S* picks have been used.

Figure 5 shows PDF maps for the first 3 sec of the evolutionary location process. The reference hypocentral location and origin time is from Fukuyama *et al.* (2003). The reference location is almost equidistant from stations SMNH01, TTRH02, and TTR007; it therefore lies near the border of the Voronoi cell of the first triggering station (SMNH01), which forms the location PDF at $\delta t = 0$ sec. One second after this first trigger ($\delta t = 1.00$ sec; $\Delta t = 2.96$ sec), both TTRH02 and TTR007 have triggered and the location PDF is now centered around the reference epicenter. After one more second, an outlier pick appears (HRS021; time error ~4.5 sec before the first arrival), but the PDF continues collapsing around the reference epicenter, and the event depth is bounded above and below. The last snapshot shows the location 3 sec after

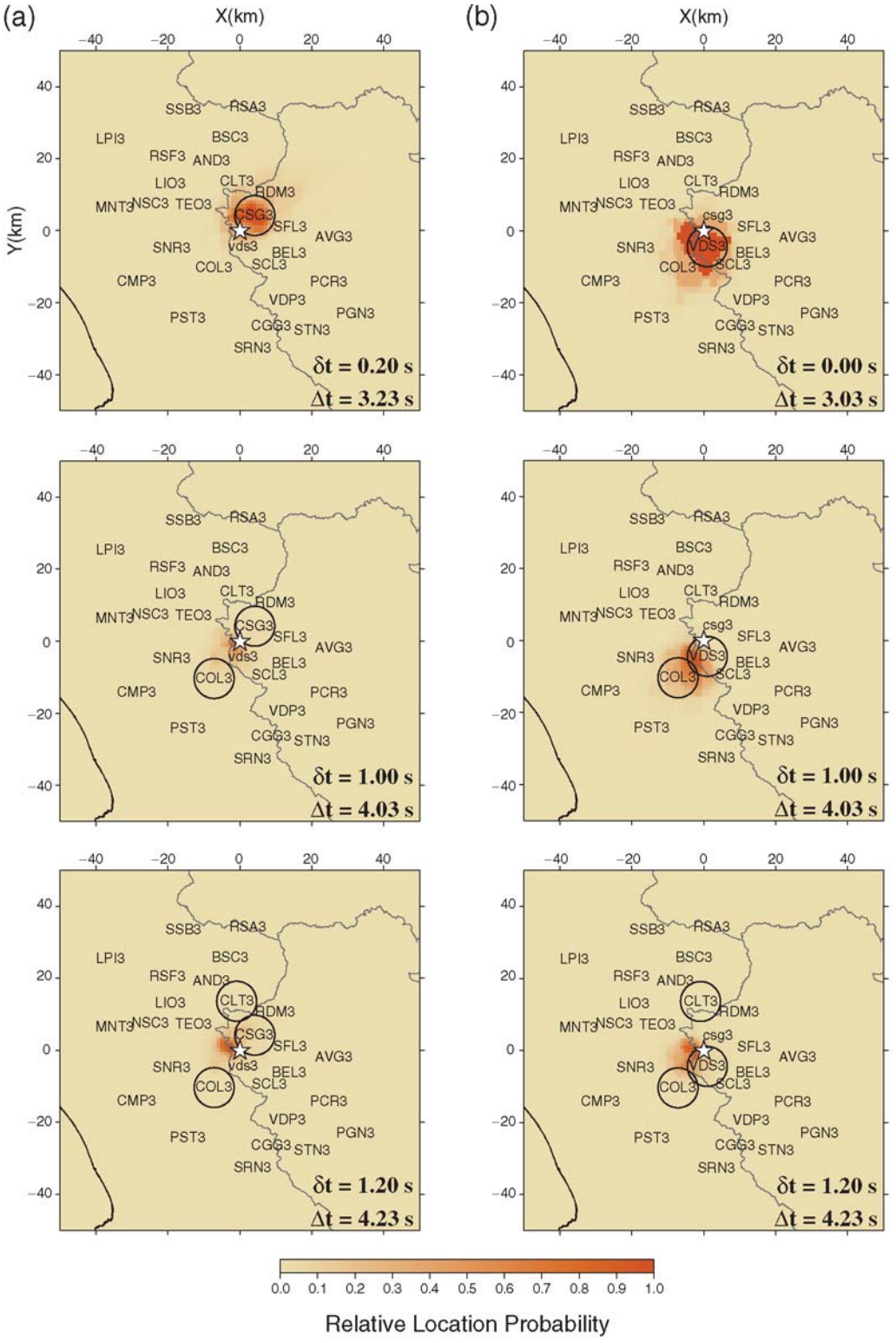

Figure 4. Synthetic location test with nontriggering stations. In column (a), the first station (VDS3) is operational, but does not trigger; in column (b), the second station (CSG3) does not detect the event. Nontriggering stations are reported lowercase; other elements as in Figure 2. For simplicity, only map views are plotted.

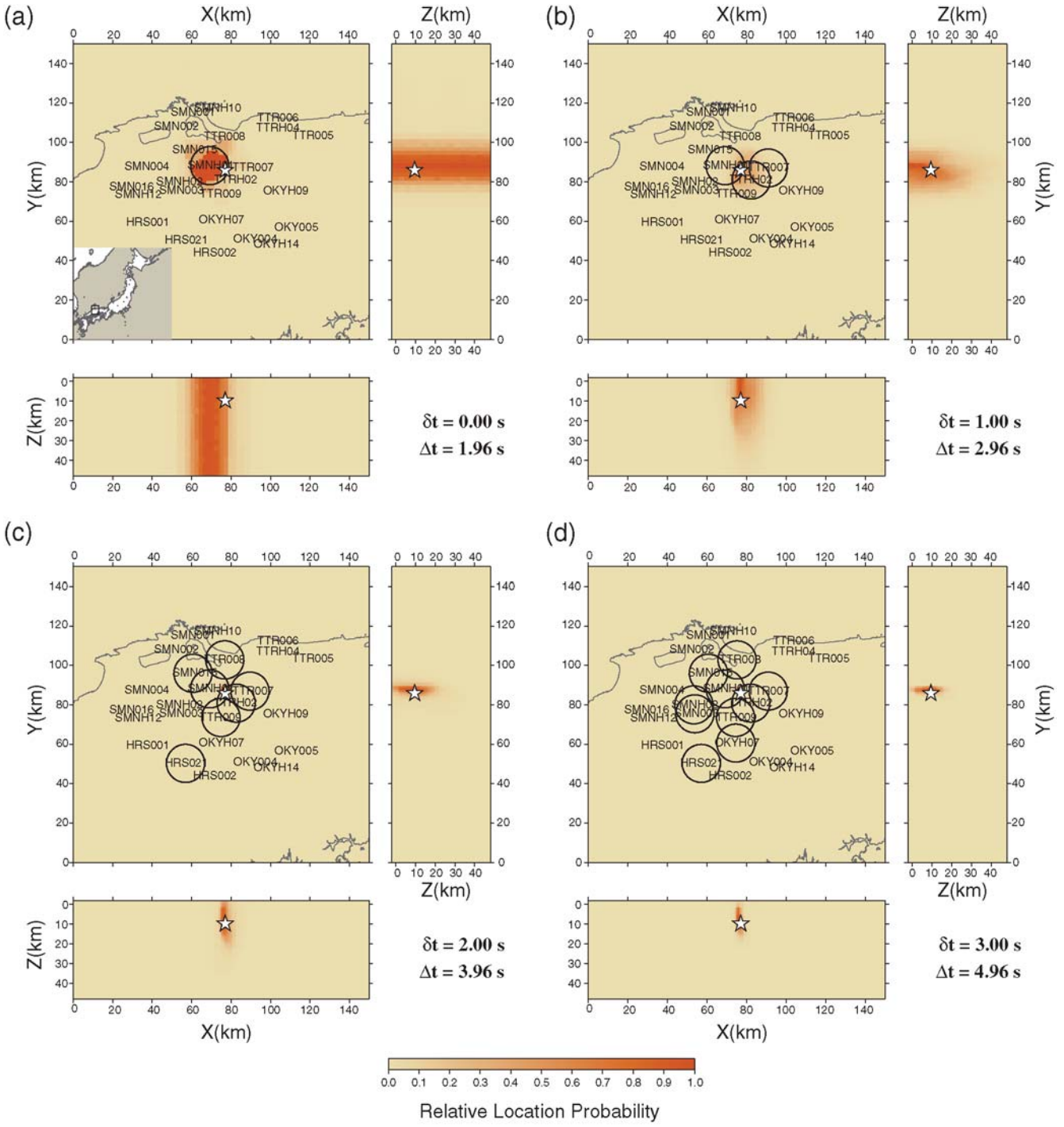

Figure 5. Simulated real-time evolutionary location for the 2000 western Tottori earthquake (M_w 6.6). The star is the location obtained by Fukuyama *et al.* (2003); other elements as in Figure 2.

the first pick ($\Delta t = 4.96$ sec) with nine triggered stations and a false trigger. The location is now well constrained in epicenter and in depth.

Real-Time Location with a Regional Network: Southern Greece

We compared the performance of our real-time location technique with respect to a non-real-time algorithm, NonLinLoc (NLL; Lomax *et al.*, 2000; Lomax, 2005). NLL is an implementation of the probabilistic formulation for earthquake location proposed by Tarantola and Vallette (1982).

In common with our real-time methodology, NLL includes the EDT formulation and the Oct-tree grid search algorithm.

A good understanding about the differences between real-time and non-real-time location can be achieved consid-

ering a regional-scale seismic network, where several seconds are needed before the ground shaking reaches three to four stations.

For this purpose, we consider an M_w 6.7 earthquake, which occurred on 8 January 2006, 195 km southwest from Athens, Greece, recorded at a seismic network with a mean station spacing of about 100 km. *P* picks at seven stations across southern Greece have been obtained from the catalog of the U.S. National Earthquake Information Center (NEIC; http://earthquake.usgs.gov/regional/neic/, last accessed March 2008) and an appropriate regional velocity model.

Figure 6 shows four location snapshots, sampled every six seconds, starting from the first trigger. In each panel, the relative real-time location probability is plotted using a color scale; the location PDF obtained using the non-real-time NLL algorithm is reported as contouring lines. Each snapshot is labeled with the time δt from the first trigger, the time Δt from the event origin, and the time t^S_{Ath} remaining for the arrival of the direct *S* wave at the city of Athens, which can be considered as the lead time available for an early-warning action (Heaton, 1985).

The first snapshot (Fig. 6a) shows the relative location probability obtained as soon as the first station (VLI) triggers at $t^S_{\mathrm{Ath}} = -40$ sec; this solution corresponds to the Voronoi cell associated to that station. The result is only mildly informative, but does show that the epicenter is likely to be south of Athens. With two triggering stations (VLI and

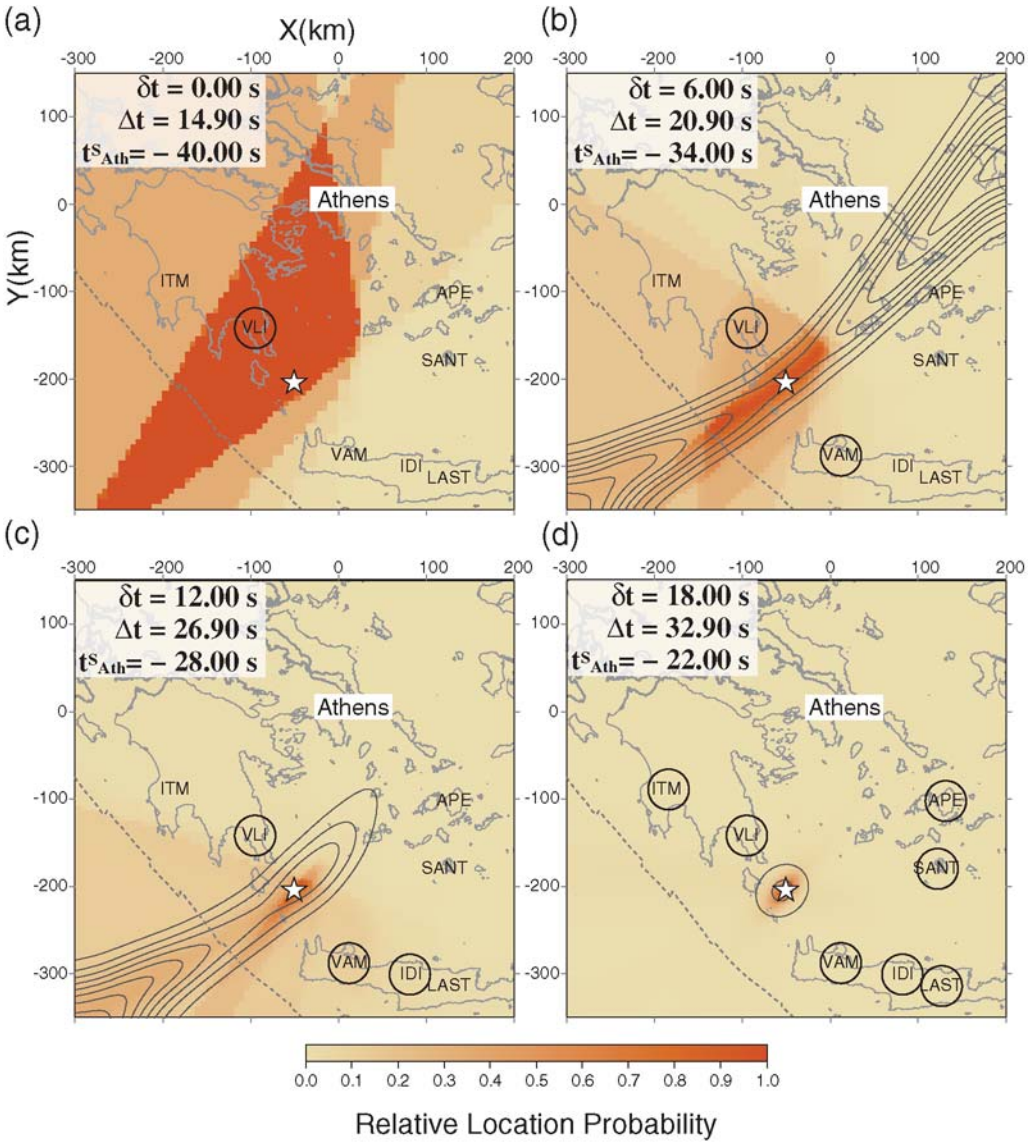

Figure 6. Simulated real-time evolutionary location for an M_w 6.7 earthquake occurred on 8 January 2006, in southern Greece. The star is the location reported in the NEIC catalog (http://earthquake.usgs.gov/regional/neic/, last accessed March 2008), and t^S_{Ath} is the time remaining for *S*-wave arrival at the city of Athens, which can be considered as the estimated lead time for an early warning at the city. The dashed line shows the trench axis of the Hellenic subduction zone, which plunges to the northeast. Other elements as in Figure 2. In panels (b), (c), and (d), the location obtained by the NLL algorithm (Lomax *et al.*, 2000) is also reported as contouring lines.

VAM, Fig 6b), at $t^S_{\mathrm{Ath}} = -34$ sec, the solution provides more useful information: the earthquake is constrained to be on the Hellenic subduction zone to the south of Greece. Beginning with two stations, location with NLL is possible. However, the NLL solution with two stations does not provide useful constraint on the epicentral area, because the location PDF is highly elongated in the southwest–northeast direction, corresponding to a single EDT surface associated to stations VLI and VAM.

With three stations available, at $t^S_{\mathrm{Ath}} = -28$ sec, the real-time location is well constrained around the true epicenter. The NLL solution, however, still retains an elongated shape and provides little useful constraint on the earthquake position. At $t^S_{\mathrm{Ath}} = -22$ sec, seven stations have recorded the first arrival, including two stations to the northeast (APE and SANT) that provide important constraint along the southwest–northeast direction. At this time, the real-time and NLL locations are similar, and both provide useful constraint on the event epicenter. Thus the real-time location procedure could provide useful early-warning information for target sites in Athens at between $t^S_{\mathrm{Ath}} = -34$ to -28 sec, while a robust nonlinear but non-real-time algorithm, NLL, could only provide useful information about 6–12 sec later, at around $t^S_{\mathrm{Ath}} = -22$ sec, out of a total *S*-wave travel time to Athens of about 55 sec.

Multiple-Event Rupture

Recently, in Italy, there have been large earthquakes characterized by multiple-event ruptures and intense seismic activity related to foreshocks and aftershocks (i.e., Friuli, 1976 [Briole *et al.*, 1986]; Irpinia, 1980 [Bernard and Zollo, 1989]; Umbria-Marche, 1997 [Amato, 1998]). The major instrumental event in the Irpinia region, the M_{w} 6.9 1980 earthquake, had multiple subevents with three main shocks occurring within about 20 sec of each other. It is therefore important for real-time location algorithms to be able to discriminate between picks coming from different events occurring with a very short delay each after the other (multiple events).

Given a list of *P*-wave arrival times, a set of stations, and a velocity model, the location method must identify the smallest set of hypocenters that could have produced the current list of arrival times. To investigate this scenario, we present a preliminary algorithm for iteratively associating arrivals with events. This algorithm is related to the one present in Earthworm Binder (Dietz, 2002), with the main differences being that we perform phase association and precise event location concurrently, using a unique location algorithm. When a new arrival-time pick is available from the station S_i, the pick is temporarily associated to each active event, and the event's relative location probability is recomputed. The reliability of the new location is checked by computing travel-time residuals at station S_i for the maximum-likelihood hypocenter $(\hat{i}, \hat{j}, \hat{k})$. Following the EDT approach, we evaluate the root mean square (rms) of differential times:

$$\mathrm{rms}_i = \sqrt{\frac{1}{M}\sum_{m=1}^{M}\left[(tt_i - tt_m)_{\hat{i},\hat{j},\hat{k}} - (t_i - t_m)\right]^2}; \qquad m \neq i, \tag{7}$$

where tt_i and tt_m are the expected travel time from the estimated hypocenter to station S_i and S_m, respectively, and t_i and t_m are the observed arrival times. The index m denotes stations that have already triggered. If rms_i is lower than a certain threshold ($\mathrm{rms}_{\max}$), the pick is associated to the event, and the new location is saved. If this condition is not fulfilled for any existing event, a new event is declared.

The value for $\mathrm{rms}_{\max}$ is related to the minimum interevent distance we can resolve. For example, considering the ISNet geometry, we expect for two events 20 km apart and for a station at the edge of the network (about 40 km away) a difference in travel time of about 1 sec (using a mean V_p of 4 km/sec). This difference becomes higher for stations closer to the event pair.

Table 2 shows the result of a synthetic test performed using the ISNet geometry (see Fig. 2 for reference) for two events occurring at $(x, y, z) = (0, 0, 10)$ and $(x, y, z) = (10, 10, 10)$, 3 sec apart. Following the rule, we chose $\mathrm{rms}_{\max} = 1.0$ sec. Arrivals from the two events are correctly detected with the exception of one single case ($\delta t = 2.40$ sec, RDM3). We note that, once the arrival time has been associated to a certain event, the location procedure is exactly the same as in the single-event case. Therefore, the resulting locations are similar to what has been shown in Figures 2 and 3.

Discussion

We have presented a probabilistic real-time evolutionary location technique based on the EDT formulation, which solves directly for the hypocenter spatial coordinates, independent of origin time, and which is highly robust in presence of outlier data. At each timestep, this algorithm makes use of both information from triggered arrivals and not-yet-triggered stations. Constraint on the hypocenter location is obtained as soon as the first station has triggered and is updated at fixed time intervals or when a new station triggers.

The hypocenter location is estimated as a PDF defined within a predefined search volume. This probabilistic description of the location results is easy to incorporate into a decision system for seismic early warning. Such a system uses a decision rule based on the probability that a ground-motion intensity value (im), such as peak ground acceleration or velocity, will exceed a given threshold at a site at which the strong shaking has not yet arrived. The PDF for im (f_{IM}) is calculated from the hazard integral, conditioned to the current estimates of magnitude and epicentral distance (Iervolino *et al.*, 2006):

$$f_{IM}(im) = \int_M \int_R f_{IM|M,R}(im|m, r) f_M(m) f_R(r)\, dm\, dr,$$

Table 2
Synthetic Phase Association Test

δt (sec)	Station Name	True Event	Detected Event	rms for Event 1	rms for Event 2
0.00	VDS3	1	1	n/a	n/a
0.20	CSG3	1	1	0.028	n/a
1.00	COL3	1	1	0.333	n/a
1.20	CLT3	1	1	0.256	n/a
1.40	SCL3	1	1	0.473	n/a
1.40	SFL3	1	1	0.375	n/a
1.80	BEL3	1	1	0.414	n/a
1.80	RDM3	1	1	0.240	n/a
1.80	TEO3	1	1	0.282	n/a
2.40	***RDM3***	***2***	***1***	***0.600***	n/a
2.60	AND3	1	1	0.301	n/a
2.60	SNR3	1	1	0.300	n/a
3.20	LIO3	1	1	0.320	n/a
3.60	BSC3	1	1	0.391	n/a
3.60	VDP3	1	1	0.248	n/a
3.60	**CLT3**	**2**	**2**	**2.228**	n/a
3.60	**CSG3**	**2**	**2**	**3.305**	**0.121**
3.80	**SFL3**	**2**	**2**	**2.218**	**0.467**
4.00	AVG3	1	1	0.397	0.467
4.00	NSC3	1	1	0.285	0.467
4.40	PST3	1	1	0.267	0.467
4.40	RSF3	1	1	0.260	0.467
4.60	CGG3	1	1	0.281	0.467
4.60	PCR3	1	1	0.239	0.467
5.00	CMP3	1	1	0.272	0.467
5.00	**BEL3**	**2**	**2**	**3.230**	**0.264**
5.20	SRN3	1	1	0.286	0.264
5.40	**VDS3**	**2**	**2**	**5.231**	**0.477**
5.60	**AND3**	**2**	**2**	**2.787**	**0.222**
5.80	RSA3	1	1	0.279	0.222
5.80	STN3	1	1	0.233	0.222
5.80	**BSC3**	**2**	**2**	**1.850**	**0.265**
5.80	**SCL3**	**2**	**2**	**4.518**	**0.183**
6.00	MNT3	1	1	0.250	0.183
6.00	**AVG3**	**2**	**2**	**2.024**	**0.236**
6.40	SSB3	1	1	0.233	0.236
6.60	**TEO3**	**2**	**2**	**4.958**	**0.235**
6.80	**COL3**	**2**	**2**	**5.464**	**0.539**
7.00	PGN3	1	1	0.216	0.539
7.20	**RSA3**	**2**	**2**	**1.435**	**0.298**
7.60	LPI3	1	1	0.307	0.298
7.60	**PCR3**	**2**	**2**	**3.154**	**0.243**
7.80	**LIO3**	**2**	**2**	**4.279**	**0.216**
7.80	**VDP3**	**2**	**2**	**4.435**	**0.228**
8.20	**RSF3**	**2**	**2**	**3.732**	**0.256**
8.40	**NSC3**	**2**	**2**	**4.504**	**0.412**
8.40	**SNR3**	**2**	**2**	**5.886**	**0.263**
8.80	**SSB3**	**2**	**2**	**2.384**	**0.240**
9.20	**CGG3**	**2**	**2**	**4.738**	**0.269**
10.00	**PGN3**	**2**	**2**	**3.184**	**0.256**
10.00	**STN3**	**2**	**2**	**4.258**	**0.198**

Synthetic phase association test for two events 14 km apart horizontally (both at 10-km depth) and 3 sec apart in time. An rms threshold of 1.0 sec was used. δt is the time from the first event detection. The first 10 sec of location are shown; picks associated to the second event are highlighted in bold. There is only one misinterpreted pick at $\delta t = 2.40$ sec for station RDM3, evidenced in italics.

where $f_{IM|M,R}$ is the attenuation law for a given strong-motion parameter, f_M is the PDF for the magnitude (estimated in real time), and f_R is the PDF for the epicentral distance, which can be obtained by simple numerical integration of the PDF output by our location technique.

Tests performed on both synthetic and real data show that when a dense seismic network (i.e., with a mean station spacing of about 10 km) is deployed around the fault zone, a location accuracy, sufficient for early-warning needs, is achieved within 1–3 sec after the first arrival detection. A further test on an earthquake recorded at a larger regional-scale network (southern Greece, mean station spacing ~100 km) demonstrates that the real-time technique can provide useful constraints on the final location 10–12 sec before a non-real-time algorithm, thus ensuring a larger lead time for early-warning actions.

A synthetic test on two quasi-simultaneous events indicates that the capability of detecting outlier data can be effectively used to identify picks coming from different events. Thus, phase association and accurate event location can be performed at the same time with a fast and reliable procedure that is particularly suited for early-warning applications.

Our real-time location technique is based on several key features used by non-real-time nonlinear procedures, including the EDT formulation, probabilistic solution, and an efficient global grid search. These features are incorporated and extended into a real-time algorithm, which includes the additional information provided by not-yet-triggered stations. It is thus to be expected, and we have demonstrated with several tests, that the real-time location algorithm inherently provides a solution that is always the same or better (e.g., faster to converge) than standard nonlinear procedures, and the real-time technique has additional advantages with respect to linearized methods (better definition of uncertainties, more robust with outliers, easily applied with 3D models; e.g., Lomax *et al.*, 2000; Husen *et al.*, 2003; Lomax, 2005). These characteristics suggest that the real-time location procedure will always provide optimal information for early warning, even if the typical gain in warning time over other procedures is expected to be small, and thus, except for certain cases where computational efficiency is paramount, the real-time procedure forms a practical and useful tool for early warning.

Acknowledgments

This research has been funded by Analisi e Monitoraggio del Rischio Ambientale: Analysis and Monitoring of Environmental Risk (AMRA scarl) through the Seismic Early Warning for Europe (SAFER) project, the EU's Sixth Framework Programme. We acknowledge and thank the National Institute of Earth Science and Disaster Prevention (NIED) for making publicly available data from K-Net and KiK-Net strong-motion networks.

References

Allen, R. (1982). Automatic phase pickers: their present use and future prospects, *Bull. Seismol. Soc. Am.* **72,** S225–S242.

Allen, R. M., and H. Kanamori (2003). The potential for earthquake early warning in southern California, *Science* **300,** 786–789.

Amato, A., R. Azzara, C. Chiarabba, G. B. Cimini, M. Cocco, M. Di Bona, L. Margheriti, S. Mazza, F. Mele, G. Selvaggi, A. Basili, E. Boschi, F. Courboulex, A. Deschamps, S. Gaffet, G. Bittarelli, L. Chiaraluce, D. Piccinini, and M. Ripepe (1998). The 1997 Umbria-Marche, Italy, earthquake sequence: a first look at the main shocks and aftershocks, *Geophys. Res. Lett.* **25,** no. 15, 2861–2864.

Bernard, P., and A. Zollo (1989). The Irpinia (Italy) 1980 earthquake: detailed analysis of a complex normal faulting, *J. Geophys. Res.* **94,** no. B2, 1631–1647.

Briole, P., G. De Natale, P. Gaulon, F. Pingue, and R. Scarpa (1986). Inversion of geodetic data and seismicity associated with the Friuli earthquake sequence (1976–1977), *Ann. Geophys.* **4,** 481–492.

Cichowicz, A. (1993). An automatic S-phase picker, *Bull. Seismol. Soc. Am.* **83,** 180–189.

Cua, G., and T. Heaton (2007). The virtual seismologist (VS) method: a Bayesian approach to earthquake early warning, in *Earthquake Early Warning Systems*, P. Gasparini, G. Manfredi and J. Zschau (Editors), Springer-Verlag, Berlin.

Dietz, L. (2002). Notes on configuring BINDER_EW: Earthworm's phase associator, http://folkworm.ceri.memphis.edu/ew-doc/ovr/binder_setup.html (last accessed March 2008).

Font, Y., H. Kao, S. Lallemand, C.-S. Liu, and L.-Y. Chiao (2004). Hypocentral determination offshore eastern Taiwan using the maximum intersection method, *Geophys. J. Int.* **158,** 655–675.

Fukuyama, E., W. L. Ellsworth, F. Waldhauser, and A. Kubo (2003). Detailed fault structure of the 2000 western Tottori, Japan, earthquake sequence, *Bull. Seismol. Soc. Am.* **93,** 1468–1478.

Heaton, T. H. (1985). A model for a seismic computerized alert network, *Science* **228,** 987–990.

Horiuchi, S., H. Negishi, K. Abe, A. Kamimura, and Y. Fujinawa (2005). An automatic processing system for broadcasting earthquake alarms, *Bull. Seismol. Soc. Am.* **95,** 708–718.

Husen, S., E. Kissling, N. Deichmann, S. Wiemer, D. Giardini, and M. Baer (2003). Probabilistic earthquake location in complex three-dimensional velocity models: application to Switzerland, *J. Geophys. Res.* **108,** no. B2, 2077, doi 10.1029/2002JB001778.

Iervolino, I., V. Convertito, M. Giorgio, G. Manfredi, and A. Zollo (2006). Real-time risk analysis for hybrid earthquake early warning systems, *J. Earthq. Eng.* **10,** no. 6, 867–885.

Kanamori, H. (2005). Real-time seismology and earthquake damage mitigation, *Ann. Rev. Earth Planet. Sci.* **33,** 195–214.

Lee, W. H. K., and J. M. Espinosa-Aranda (2003). Earthquake early warning systems: current status and perspectives, in *Early Warning Systems for Natural Disaster Reduction*, J. Zscahu and A. N. Kuppers (Editors), Springer, Berlin, 409–423.

Lomax, A. (2005). A reanalysis of the hypocentral location and related observations for the great 1906 California earthquake, *Bull. Seismol. Soc. Am.* **95,** 861–877.

Lomax, A., and A. Curtis (2001). Fast, probabilistic earthquake location in 3D models using Oct-tree importance sampling, *Geopys. Res. Abstr.* **3,** 955.

Lomax, A., J. Virieux, P. Volant, and C. Berge (2000). Probabilistic earthquake location in 3D and layered models: introduction of a Metropolis-Gibbs method and comparison with linear locations, in *Advances in Seismic Event Location*, C. H. Thurber and N. Rabinowitz (Editors), Kluwer, Amsterdam, 101–134.

Magotra, N., N. Ahmed, and E. Chael (1987). Seismic event detection and source location using single station (three-component) data, *Bull. Seismol. Soc. Am.* **77,** 958–971.

Milne, J. (1886). *Earthquakes and Other Earth Movements*, Appelton, New York, 361 pp.

Podvin, P., and I. Lecomte (1991). Finite difference computations of traveltimes in very contrasted velocity models: a massively parallel approach and its associated tools, *Geophys. J. Int.* **105,** 271–284.

Rydelek, P., and J. Pujol (2004). Real-time seismic warning with a 2-station subarray, *Bull. Seismol. Soc. Am.* **94,** 1546–1550.

Tarantola, A., and B. Vallette (1982). Inverse problems=quest for information, *J. Geophys.* **50,** 159–170.

Weber, E., V. Convertito, G. Iannaccone, A. Zollo, A. Bobbio, L. Cantore, M. Corciulo, M. Di Crosta, L. Elia, C. Martino, A. Romeo, and C. Satriano (2007). An advanced seismic network in the Southern Apennines (Italy) for seismicity investigations and experimentation with earthquake early warning, *Seism. Res. Lett.* **78,** no. 6, 622–634, doi 10.1785/gssrl.78.6.622.

Weisstein, E. W. (1999). Voronoi polygon, in *MathWorld: A Wolfram Web Resource*, http://mathworld.wolfram.com/VoronoiPolygon.html (last accessed March 2008).

Withers, M., R. Aster, C. Young, J. Beiriger, M. Harris, S. Moore, and J. Trujillo (1998). A comparison of select trigger algorithms for automated global seismic phase and event detection, *Bull. Seismol. Soc. Am.* **88,** 95–106.

Zhou, H. (1994). Rapid 3-D hypocentral determination using a master station method, *J. Geophys. Res.* **99,** 15,439–15,455.

Zollo, A., M. Lancieri, and S. Nielsen (2006). Earthquake magnitude estimation from peak amplitudes of very early seismic signals on strong motion records, *Geophys. Res. Lett.* **33,** L233112, doi 10.1029/2006GL027795.

RISSC-Lab, AMRA scarl
Via Diocleziano 328
80124 Napoli, Italy
satriano@na.infn.it
(C.S.)

ALomax Scientific, Mouans-Sartoux, France
161 Allée du Micocoulier
06370 Mouans-Sartoux, France
anthony@alomax.net
(A.L.)

RISSC-Lab, Dipartimento di Scienze Fisiche
Università di Napoli Federico II
Via Diocleziano 328
80124 Napoli, Italy
aldo.zollo@unina.it
(A.Z.)

Manuscript received 18 July 2006